ADVANCED MATERIALS TECHNOLOGIES
www.advmattechnol.de

MXene-Polymer Hybrid for High-Performance Gas Sensor Prepared by Microwave-Assisted In-Situ Intercalation

Jin Zhou, Seyed Hossein Hosseini Shokouh, Hannu-Pekka Komsa, Lassi Rieppo, Linfan Cui, Zhong-Peng Lv, and Krisztian Kordas**

2D transition-metal carbides ($Ti_3C_2T_x$ MXene) intercalated with organic molecules have been widely used in batteries and supercapacitors, but are quite rarely reported for gas sensing. Since $Ti_3C_2T_x$ is sensitive to oxygen, most methods for preparing the intercalated $Ti_3C_2T_x$ involve stirring the reactants with $Ti_3C_2T_x$ for several hours under nitrogen protection. Herein, a method to prepare a hybrid of $Ti_3C_2T_x$ and intercalated polysquaraine through microwave-assisted in situ polymerization that takes only a few minutes without the need of using a protective atmosphere is demonstrated. Owing to the increased interlayer space of the $Ti_3C_2T_x$ after the polymerization, the gas sensors based on the hybrid exhibit a good sensing performance for NH_3 detection, being able to detect at least 500 ppb NH_3 with a 2.2% ppm^{-1} of sensitivity. This study provides a facile preparation method for developing intercalated MXenes, which are expected to be useful for a wide range of applications.

1. Introduction

MXenes are members of the family of 2D materials, which are typically formed by selectively etching the intermediate A layers from the MAX phase as first reported in 2011.[1] MXenes generally have the formula of $M_{n+1}X_nT_x$, where M is an early transition metal, X is carbon or nitrogen, and T_x represents surface terminating functional groups such as –F, –O, and –OH.[1] Owing to its fascinating surface properties, metallic conductivity, and hydrophilicity, MXenes have been proposed for applications in energy storage,[2,3] catalysis,[4,5] electromagnetic interference shielding,[6,7] and sensing.[8–11] Recently, MXenes and their derivatives have been noted to be useful for gas sensing, e.g., NH_3 and volatile organic compounds (VOCs).[10,12–14] However, the response of pristine MXene-based gas sensors is typically low (e.g., 0.62% for 10 ppm NH_3)[15] and their limit of detection is high as compared to metal oxide and organic semiconductor-based devices, which limit their practical applications. [12,14,15]

Hybridizing MXenes with other sensitive materials is one strategy to overcome or at least minimize these challenges. Intercalation of molecules between MXene sheets in the composites/hybrids can provide a large interlayer spacing and facilitate rapid ion transport,[16] as has been exploited in novel ion batteries[17] and supercapacitors.[18–21] The presence of multiple interfaces between materials having different electronic band structures may significantly alter the electrical transport as well as the surface adsorption energy and the density of active sites.[22–29] Intercalation was also found to improve the selectivity of gas sensors,[30] and to influence the dynamics of interlayer water of MXene with an important role in the sensing process.[31,32] Among these hybrids/composites, sensors made of MXenes and organic composites, such as polyaniline,[24,33] polyacrylamide,[22] PEDOT: PSS,[25] and polyethyleneimine,[23] exhibit rather a good sensing performance.

Interestingly, most of the efforts in gas sensor applications of MXene-based composites were obtained by simple physical blending, while only very few studies have considered intercalation.[34] Different preparation recipes proposed for intercalation of MXenes with organic materials, often suffer from long reaction times at elevated temperatures, which is energy demanding, and eventually may accelerate oxidation.[9] For example, Boota et al. intercalated polymers of various polarities into MXene layers by stirring the mixture of reactants and MXenes for 16 h at 80 °C under nitrogen atmosphere.[35] Also, they intercalated MXenes with polypyrrole through the self-polymerization of pyrrole at room temperature under 12 h stirring.[20] Overbury

J. Zhou, S. H. Hosseini Shokouh, H.-P. Komsa, K. Kordas
Microelectronics Research Unit
Faculty of Information Technology and Electrical Engineering
University of Oulu
P.O. Box 4500, Oulu FIN-90014, Finland
E-mail: krisztian.kordas@oulu.fi

L. Rieppo
Research Unit of Medical Imaging
Physics and Technology
Faculty of Medicine
University of Oulu
Oulu FIN-90014, Finland

L. Cui
Department of Electronics and Nanoengineering
Aalto University
Aalto FIN-00076, Finland

Z.-P. Lv
Department of Applied Physics
Aalto University
Aalto FIN-00076, Finland
E-mail: zhongpeng.lyu@aalto.fi

The ORCID identification number(s) for the author(s) of this article can be found under https://doi.org/10.1002/admt.202101565.

DOI: 10.1002/admt.202101565

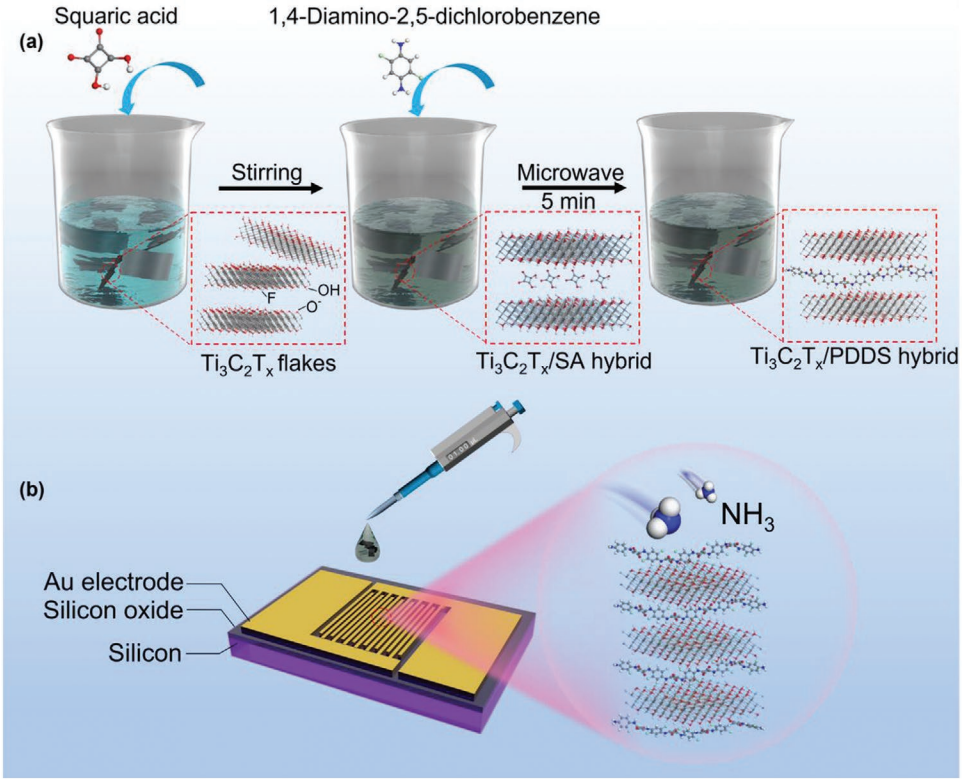

Figure 1. a) Schematic illustration of polymerization of squaric acid (SA) and 1,4-diamino-2,5-dichlorobenzene between $Ti_3C_2T_x$ layers. b) The chemiresistive NH_3 sensor device based on a $Ti_3C_2T_x$/PDDS hybrid film after drop-coat on the electrodes.

et al. stirred MXene and urea solution for 15 h at 60 °C to prepare the corresponding intercalated product.[36]

Herein, we demonstrate a novel, fast and highly efficient microwave-assisted synthetic route for preparing intercalated $Ti_3C_2T_x$/polymer hybrids. The excellent microwave absorption of $Ti_3C_2T_x$ can largely accelerate the polymerization process.[37,38] Under only 5 min microwave radiation, a new conjugated polysquaraine, poly-(1,4-diamino-2,5-dichlorobenzene-squarine) (PDDS) with a backbone containing ionic-state moieties, formed in-situ and intercalated between the layers of $Ti_3C_2T_x$ with a controlled ratio. Polysquaraine was first developed by Xiao et al. for gas sensing by refluxing and stirring squaric acid with an aromatic amine at 125 °C for 12 h.[39] Due to the zwitterionic resonance (N^+ and O^-) structure of the squaric ring and an arylamine, squaraines can form hydrogen bonds and/or participate in ion-dipole interactions upon exposure to target gases.[39–42] However, their typically poor conductivity may limit practical applications. The use of metallic $Ti_3C_2T_x$ in our hybrids also led to significantly enhanced conductivity, therefore circumventing this problem. Our sensors based on $Ti_3C_2T_x$/PDDS hybrid provided superior response compared to pristine $Ti_3C_2T_x$ and simple physical mixture of $Ti_3C_2T_x$ and PDDS, detecting NH_3 with a sensitivity of 2.2% ppm^{-1} at 500 ppb and exhibiting good selectivity and repeatability.

2. Results and Discussion

To prepare the $Ti_3C_2T_x$/PDDS hybrid material (**Figure 1**), a colloidal aqueous $Ti_3C_2T_x$ was stirred with squaric acid (SA) in three different mass ratios ($Ti_3C_2T_x$: SA = 1:1, 1:2, and 1:5). Then, the $Ti_3C_2T_x$/SA hybrid was washed with deionized water and reacted with 1,4-diamino-2,5-dichlorobenzene in *n*-butanol for 5 min under microwave exposure (see experimental details). After washing with water and acetone, the product was dried and finally suspended in ethanol to allow for drop-cast deposition on the substrate with the interdigital electrodes (see Experimental Section). To quantify the PDDS in the $Ti_3C_2T_x$/PDDS hybrid, we conducted thermogravimetric analyses (TGA) of the hybrids, pristine $Ti_3C_2T_x$ and PDDS (Figure S1, Supporting Information). The amount of the PDDS in the hybrids increases with the amount of SA used, and the mass ratio of PDDS in the $Ti_3C_2T_x$/SA (1:1), (1:2), and (1:5) samples is calculated to be 4%, 30% and 35%, respectively. We, therefore, denoted the three samples as MP 4%, MP 30%, and MP 35% in our study.

Upon drop-casting the $Ti_3C_2T_x$/PDDS hybrid (MP 30%) on the substrate, nanosheet structures (of about 2.5 μm in length and width) that percolate and bridge the adjacent electrodes are visible by scanning electron microscopy imaging (**Figure 2**a). Transmission electron microscopy (TEM) shows the PDDS (bright layers) is confined between $Ti_3C_2T_x$ layers (dark layers), leading to the increase of their interlayer distance (Figure 2b). Energy-dispersive X-ray spectroscopy (EDS) mapping in Figure S2 (Supporting Information) confirms the uniform distribution of PDDS in the hybrid. In particular, the nitrogen element distributes homogeneously over the surface of $Ti_3C_2T_x$ layers, suggesting a uniform distribution of PDDS throughout the hybrid, which agrees with TEM results. Powder X-ray diffraction (XRD) pattern (Figure 2c) of the pristine $Ti_3C_2T_x$ and the $Ti_3C_2T_x$/PDDS hybrid exhibits a clear shift of the (002)

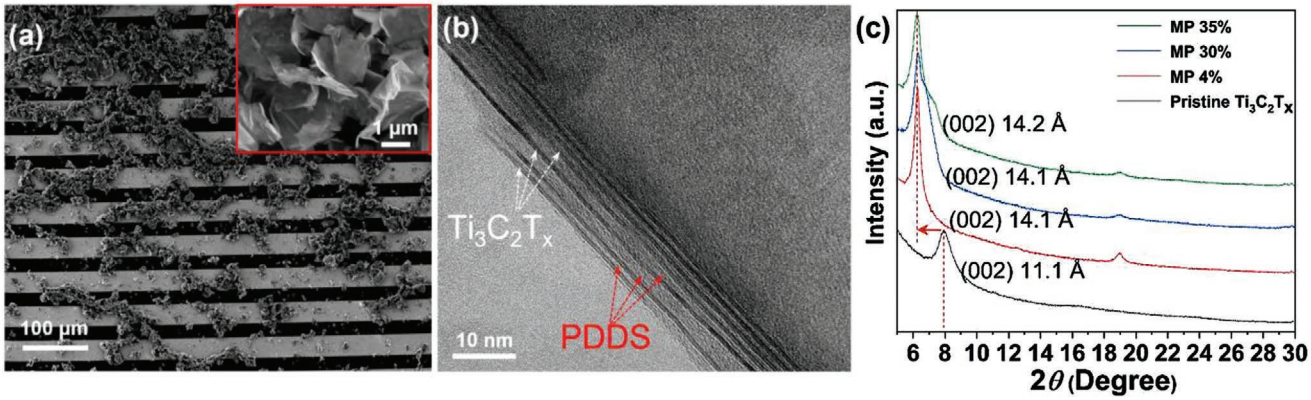

Figure 2. a) SEM image of the sensor device fabricated from MP 30%; inset: a magnified image of the flakes. b) TEM image of MP 30%, PDDS (bright layers) is intercalated between the $Ti_3C_2T_x$ layers (darker layers); c) XRD pattern of $Ti_3C_2T_x$/PDDS hybrids and pristine $Ti_3C_2T_x$. The interlayer spacings deduced from the (002) peak position are also indicated.

reflection from 7.96° to 6.26°, 6.26°, and 6.24° as the amount of SA is increased, further indicating an expansion of the *d* space between $Ti_3C_2T_x$ layers from 11.1 to 14.2 Å. The $Ti_3C_2T_x$ interlayer distance expansion can be attributed to the presence of the polymer between the $Ti_3C_2T_x$ layers. The interlayer distance of $Ti_3C_2T_x$/SA hybrid (Figure S3a, Supporting Information) is 12.0 Å, i.e., falling between those of the pure $Ti_3C_2T_x$ and the $Ti_3C_2T_x$/PDDS hybrid, and thus indicates successful polymerization of the intercalated SA. It is worth noting that benefiting from the ion-in-conjugated structure of PDDS (Figure S4, Supporting Information), the large polarity of the polymer promotes strong the interaction between polymer and $Ti_3C_2T_x$, which is in agreement with the report of Boota and coworkers.[32] The stronger the interaction between the polymer and $Ti_3C_2T_x$, the more polymer could be retained between $Ti_3C_2T_x$ flakes after washing, which results in an increased interlayer distance for $Ti_3C_2T_x$. Interestingly, when the polymer is in excess, a shoulder at the (002) reflection is visible, which cannot be a direct peak of the polymer (Figure S3b, Supporting Information). It may originate from the secondary layered product. Moreover, the $Ti_3C_2T_x$ layers could work as a template or a substrate for the synthesis due to the H-binding between $Ti_3C_2T_x$ and the monomers or PDDS oligomers and thus facilitate layered polymerization.[20,43]

The Fourier transform infrared (FTIR) spectrum of MP 30% (**Figure 3**a) exhibits clear characteristic peaks of PDDS superposed on the spectrum of $Ti_3C_2T_x$. Compared to the pristine $Ti_3C_2T_x$, the spectrum of $Ti_3C_2T_x$/PDDS hybrid shows peaks originating from the zwitterionic structure of cyclobutenediylium-1,3-diolate and C=C stretching of the four-membered ring of PDDS at 1627 and 1508 cm^{-1}, respectively.[44,45] Similar spectra can also be found in the case of MP 4% and MP 35% as shown in Figure S5a (Supporting Information). The Raman spectrum of $Ti_3C_2T_x$/PDDS (Figure 3b) further corroborates the formation of PDDS. The peaks at 1238, 1362, 1523, and 1790 cm^{-1} are from the intercalated PDDS. Specifically, the peaks at 1523 and 1790 cm^{-1} can be assigned to the Ph C-C and C=C stretching of the four-membered ring combinations and symmetrical C–O combinations in PDDS.[46] The Raman bands observed at 126, 202, 601 and 723 cm^{-1} are associated with the resonance peak, A_{1g} (Ti, O, C), M–T_x, and A_{1g}(C) peaks in $Ti_3C_2T_x$, respectively.[47] Moreover, the lack of peaks related to TiO_x in the spectrum indicates that $Ti_3C_2T_x$ is not oxidized during the fast polymerization process nor after it, likely due to the protection by PDDS.[9] The Raman spectrum of MP 35% hybrid shows very similar features (Figure S5b, Supporting Information), whereas MP 4% hybrid appears close to pristine $Ti_3C_2T_x$, consistent with its very small PDDS mass content of 4% estimated from TGA. It is important

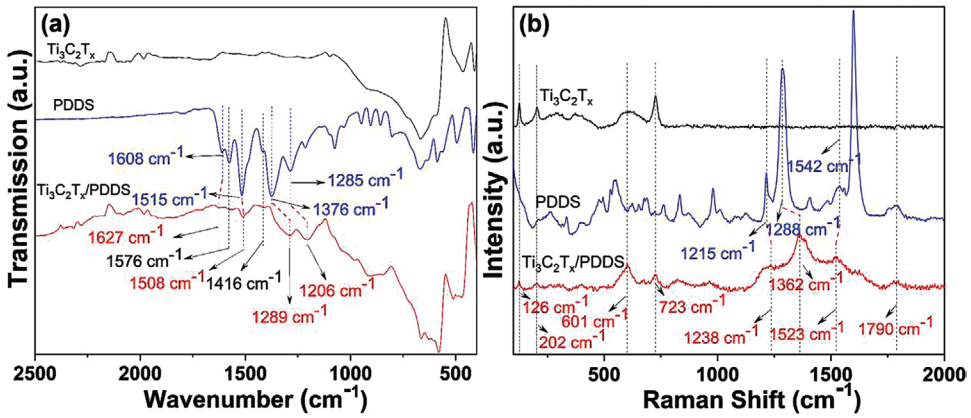

Figure 3. a) FTIR spectra and b) Raman spectra of $Ti_3C_2T_x$ (black curve), PDDS (blue curve), and $Ti_3C_2T_x$/PDDS hybrid (MP 30%) (red curve).

to note that the shifts of the FTIR and Raman peaks indicate noticable interaction between PDDS and $Ti_3C_2T_x$,[35] which plays a crucial role in the polymerization of PDDS on the surface of $Ti_3C_2T_x$. To further verify the presence of interaction between $Ti_3C_2T_x$ and PDDS prepared by in-situ polymerization, we measured the FTIR and Raman spectra of a simple mixture of PDDS and $Ti_3C_2T_x$ with a mass ratio of 1:1 (Figure S5, Supporting Information). Since the IR absorption of PDDS is significantly stronger than that of $Ti_3C_2T_x$, the FTIR spectrum of the mixture resembles that of PDDS with identical vibrational mode frequencies. The Raman spectrum of the mixture merely shows a simple combination of PDDS and $Ti_3C_2T_x$ spectra, where the widened peak of the polymer might be caused by the polymer carbonization under the laser. Moreover, we observe the separation of phases in the aqueous mixture of $Ti_3C_2T_x$ and PDDS after standing, whereas $Ti_3C_2T_x$/PDDS hybrid remains evenly dispersed in water, which further proves the presence of the interaction (Figure S6, Supporting Information).

From these results, we can conclude that our $Ti_3C_2T_x$/PDDS hybrids indeed consist of $Ti_3C_2T_x$ and PDDS, which are bound together strongly and intermixed at the atomic scale. Finally, X-ray photoelectron spectra (XPS) of $Ti_3C_2T_x$ and MP 30% are shown in Figure S7 (Supporting Information). The new N1s peak in the case of MP 30% corresponds to the –NH–[48] and $-HN^+=$[49] of PDDS (Figure S7b, Supporting Information). Furthermore, the spectrum of C 1s reveals aromatic C, C–O, C–N, and C–Cl peaks in the $Ti_3C_2T_x$/PDDS hybrid after polymerization.[35,50] These results suggest that SA and 1,4-diamino-2,5-dichlorobenzene are successfully polycondensed in contact with $Ti_3C_2T_x$ by microwave irradiation without long term refluxing.

To evaluate the sensing performance of our $Ti_3C_2T_x$/PDDS hybrids, we prepared sensor devices by drop-casting the hybrid on the silicon substrate with patterned gold interdigitated electrodes. Changes in the electrical resistance were investigated under exposures to different gases, such as H_2, CO, CH_4, H_2S, NH_3, and NO, at room temperature (25 °C). The sensor based on the MP 30% shows high selectivity toward NH_3 (**Figure 4**a; Figure S8, Supporting Information). The sensitivity of the device to NH_3 is 2.2% ppm^{-1} at 500 ppb. Although this value is inferior compared to metal oxide (including commercial sensors, Figaro TGS 826 and Winsen MQ 137) and some conductive polymer-based devices, it is surpassing previously reported MXene-based sensing materials. In terms of the practical detection limit, our sensor outperforms other MXene based devices, and even without the need of heating, it competes with metal oxide sensors (including commercial ones) (**Table 1**). Compared to the interference gases introduced in large concentrations, except for the NO, which we will discuss later in the text, the response of the sensor to 1 ppm NH_3 is at least sixfold (Figure 4a and Figure S8, Supporting Information). The sensor based on the MP 4% and MP 35% showed qualitatively similar performance, as demonstrated in Figure S9 (Supporting Information), but with lower sensitivities of 1.0% ppm^{-1} and 1.1% ppm^{-1} at 500 ppb NH_3, respectively.

The real-time sensing response curve (Figure 4b) shows how the resistance of the device is changing when exposed to NH_3 pulses from 500 ppb to 10 ppm. The resistance increases rapidly when the sensor is exposed to the analyte and then gradually recovers upon flushing with dry air. Figure 4c displays the concentration-dependent sensing response calculated

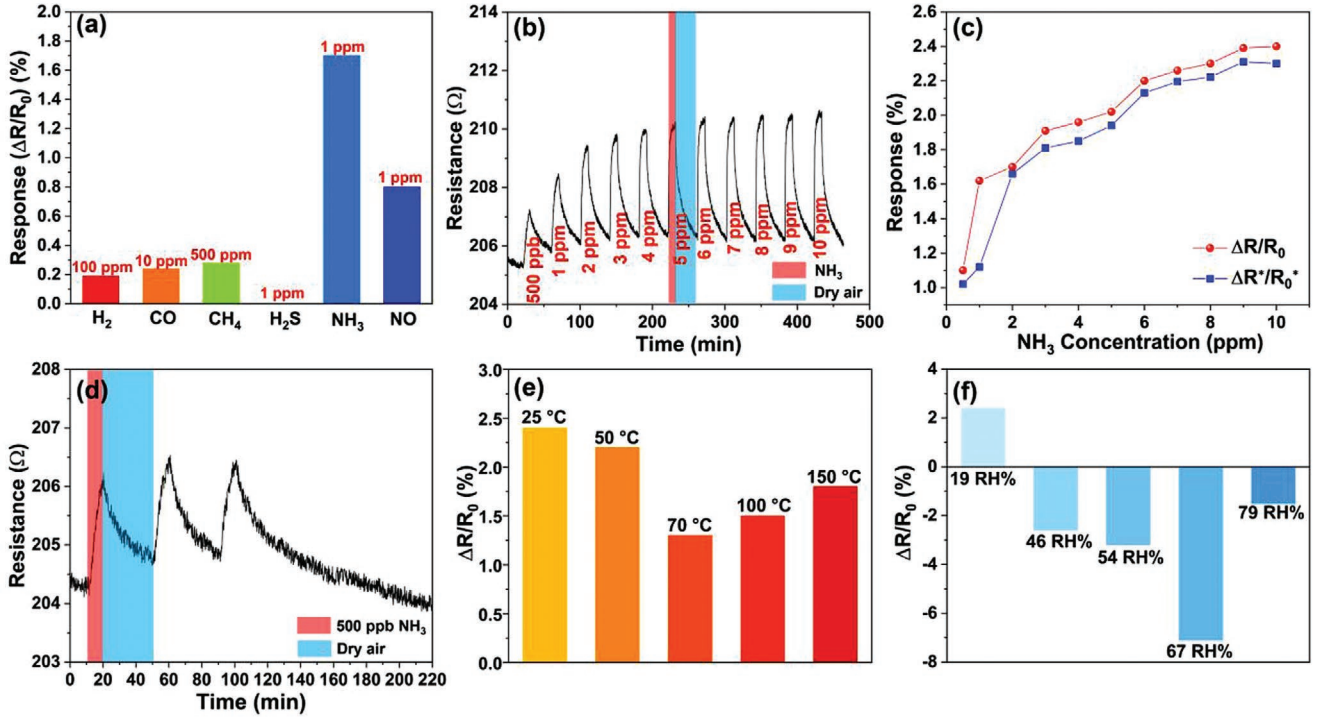

Figure 4. Sensing performances of MP 30%. a) The selectivity of the sensor; b) the real-time resistance of the sensor versus time curve; c) response at NH_3 concentrations from 0.5 to 10 ppm, $\Delta R/R_0$ and $\Delta R^*/R_0^*$ indicates the uncalibirated and calibrated response respectively; d) repeatability of the sensor at 500 ppb NH_3. The effect of e) temperature and f) humidity on the sensing performance for 10 ppm NH_3.

Table 1. Comparison of ammonia sensing performances of the gas sensors based on the MXene and the related composites/hybrids.

Material	Sensitivity [% ppm^{-1}]	LOD[a] [ppm]	Work temperature	Reference
$Ti_3C_2T_x$	0.0062	10	RT[b]	[15]
$Ti_3C_2T_x$	0.008	0.1	RT	[12]
$Ti_3C_2T_x$	0.0021	10	RT	[13]
$Ti_3C_2T_x$/rGO	0.13	10	RT	[27]
PEDOT:PSS@ $Ti_3C_2T_x$	0.96	10	RT	[34]
$Ti_3C_2T_x$/NaCl	0.012	10	RT	[51]
$Ti_3C_2T_x$/CuO	0.068	1	RT	[52]
TiO_2/$Ti_3C_2T_x$	0.31	0.5	RT	[26]
BG/Ti_3CN	0.0013	10	RT	[53]
$Ti_3C_2T_x$/SnO_2	0.8	0.5	RT	[54]
TiO_2/Ti_2CT_x	3	0.1	RT	[55]
ZnO/Graphene	−7.6	1	RT	[56]
CeO_2–CuBr	2000	0.02	RT	[57]
Polypyrrole nanotubes	40000	0.00005	RT	[58]
PANI/MoS_2/SnO_2	10	0.2	RT	[59]
Commercial NH_3 sensor (*Winsen* MQ-137)	−0.4	5	250 °C	[60]
Commercial NH_3 sensor (*Figaro TGS 826*)	55	30	RT	[61]
$Ti_3C_2T_x$/PDDS	2.2	0.5	RT	This work

[a]Limit of detection; [b]Room temperature.

from the measurements of every single concentration with ($\Delta R^*/R_0^*$) and without ($\Delta R/R_0$) calibration of the baseline drift (Figures S10 and S11a, Supporting Information). The sensor response tends to saturate at 3.3% as the NH_3 concentration increases to 20 ppm, suggesting a Langmuir type adsorption of the gas on the surface (Figure S11b, Supporting Information). To investigate the stability of the sensor after long exposure, experiments with an extended exposure time of 1 h were conducted (Figure S12, Supporting Information). A reduced response (from 2.6% to 2.2%) can be observed after a long time of NH_3 exposure, which might be ascribed to the incomplete recovery of the active sites after previous gas pulses and purging. The $Ti_3C_2T_x$/PDDS based sensor shows an acceptable level of repeatability to sequential exposure of 500 ppb NH_3 gas. For three successive cycles as shown in Figure 4d, the sensor response is similar with minimal variation (standard deviation = 0.15%). Figure S13 (Supporting Information) shows similar repeatability curves to sequential exposure of NH_3 gas at 500 ppb, 5 ppm and 10 ppm. To demonstrate the time-stability of the device, we stored the sensor in a normal indoor environment for a period of 14 days, and the repeated measurements showed nearly identical responses (Figure S14. Supporting Information).

To study the effect of working temperature on the sensing performance, we investigated the sensing response for 10 ppm NH_3 at 50, 70, 100, and 150 °C (Figure 4e). The sensor response decayed at higher working temperatures, which can be attributed to the reduced adsorption and enhanced desorption of the analyte at the active sites. Interestingly, with the temperature increased further, the sensor response increased from 1.3% at 70 °C to 1.5% at 100 °C, which might be caused by the oxidation of $Ti_3C_2T_x$.[9] Furthermore, increased humidity of the air carrier gas seems to decrease the sensor response to ammonia (Figure 4f) possibly due to the consumption of the analyte through the formation of NH_4OH.[62,63]

While pristine $Ti_3C_2T_x$ has excellent electrical conductivity, its resistance remains almost constant when exposed to NH_3 (Figure S15, Supporting Information). On the other hand, the sensory response of pristine polymer could not be measured due to its poor electrical conductivity. Accordingly, the good sensing performance achieved by the intercalation of PDDS between $Ti_3C_2T_x$ layers clearly demonstrates the synergistic effect present for the hybrid material.

The good NH_3 sensing performance of the hybrid material can be ascribed to several reasons. First, $Ti_3C_2T_x$ was reported to possess the largest charge transfer and adsorption energy when exposed to NH_3 due to the rich surface functional groups (–O, –F and –OH).[64] Second, PDDS introduces additional active sites for adsorption owing to its zwitterionic resonance (N^+ and O^-) structure that enables H-bond formation as well as ion-dipole interaction with NH_3[39,65] and thereby may also contribute to the sensor response.[39,42] Third, the enlarged interlayer spacing enables easier access to the adsorption sites between the layers for the analyte, thus making the sensor more sensitive to analytes.[30] To verify our assumptions on the positive influence of intercalation, we carried out a control experiment with a physical mixture of PDDS and $Ti_3C_2T_x$, which exhibited a sensor response of only 0.25% at 10 ppm NH_3 (Figure S16, Supporting Information).

Furthermore, as noted earlier, the exposure of the $Ti_3C_2T_x$/PDDS hybrid to NO results in a good sensory response, which is consistent with previous reports and can be explained by the relatively large adsorption energy and charge transfer between NO and $Ti_3C_2T_x$ as well as PDDS.[15,40,42] The real-time sensing

curves show increased response with the concentration of applied NO gas pulses (Figure S17, Supporting Information), although it is not linear.

3. Conclusion

In conclusion, we have demonstrated a facile and efficient strategy for the in situ polymerization of squaric acid and 1,4-diamino-2,5-dichlorobenzene between the layeres of $Ti_3C_2T_x$ by microwave irradiation. FTIR and Raman measurements confirmed the polymerization of squaric acid and 1,4-diamino-2,5-dichlorobenzene, and the XRD and TEM results proved the polymer intercalated into the $Ti_3C_2T_x$ layers, resulting in enlarged interlayer spacing. Furthermore, as the microwaves cause only a very short local temperature rise in the reaction mixture, one may avoid the oxidation of $Ti_3C_2T_x$ without applying any protective gas atmosphere during polymerization. The sensors based on $Ti_3C_2T_x$/PDDS hybrid showed good gas-sensing performance with a sensitivity of 2.2% ppm^{-1} to NH_3, which is superior to that of pristine $Ti_3C_2T_x$ and most of the reported MXene-based gas sensors. Accordingly, we believe that our strategy of using microwave-assisted polymerization and simultaneous intercalation will motivate further research on $Ti_3C_2T_x$/polymer hybrids with potential gas sensing and energy-related applications.

4. Experimental Section

Materials and Characterization: All the chemicals were ordered from Sigma Aldrich. X-ray photoelectron spectroscopy (XPS) measurements were performed with a Thermo Fisher Scientific Escalab 250 XI system with an Al Kα source. Raman spectra was performed by Thermo Scientific DXR2xi Raman imaging microscope (excitation wavelength, λ = 785 nm). The microstructure of synthesized material was studied by field-emission scanning electron microscopy (FESEM, Zeiss ULTRA plus and equipped with EDX) and transmission electron microscopy (TEM, JEOL JEM-2200FS EFTEM/STEM 200 kV). Fourier transform infrared spectroscopy (FTIR) of MXene-polymer hybrid was performed on a Spectrum Two FT-IR spectrometer with ATR model (PerkinElmer, UK). The X-ray diffraction (XRD) was carried out by Rigaku Smart Lab 9 kW, Cu Kα-radiation with a 0.02 degree of step width. The thermal gravimetric analysis (TGA, Setaram Labsys) was carried out with 10 °C min^{-1} from room temperature to 800 °C under carrier gas of air.

Synthesis of $Ti_3C_2T_x$: Aqueous dispersion of $Ti_3C_2T_x$ was synthesized using the MILD method with minor modification.[66] In a typical synthesis, 2 g Ti_3AlC_2 (325 mesh, Carbon-Ukraine) was added gradually to a stirring mixture of 40 mL 9 M HCl and 2 g LiF at 35 °C. After 24 h, the product was separated by centrifuge and washed with deionized water until pH > 5. Forty milliliters of water was then added to the sediment and vortex for 30 min. The supernatant contained few and multiple layered $Ti_3C_2T_x$ was obtained by centrifuging the mixture at 3500 rpm for 15 min and then stored at 4 °C before use. The concentration was measured by weighing a vacuum dried self-standing film of a certain volume of the $Ti_3C_2T_x$ dispersion.

$Ti_3C_2T_x$/PDDS Hybrid Preparation: To prepare the $Ti_3C_2T_x$/PDDS hybrid, 50 mL aqueous dispersion of $Ti_3C_2T_x$ (1 mg mL^{-1}) was initially bath sonicated with squaric acid (it is water soluble) for 30 min under N_2 protection. After 2 h of stirring at room temperature, the $Ti_3C_2T_x$/squaric acid mixture was washed by adding deionized water and centrifugation for 10 min at 3500 rpm three times and then washed with n-butanol once with the same condition. After transferring the $Ti_3C_2T_x$/SA mixture (a paste, containing certain parts of water and n-butanol) into 30 mL *n*-butanol with excessive 1,4-diamino-2,5-dichlorobenzene and bubbling by N_2 for 10 min, the solution was reacted under a 350-watt microwave for 5 min. Finally, the $Ti_3C_2T_x$/PDDS hybrid was washed with acetone and deionized water while vacuum filtering to ensure there was no free SA or 1,4-diamino-2,5-dichlorobenzene, and the hybrid was collected after vacuum drying at 60 °C for 8 h.

The hybrid with three mass ratios of $Ti_3C_2T_x$: SA 1:1, 1:2, and 1:5 were synthesized by changing the SA content (e.g., when the mass ratios of $Ti_3C_2T_x$: SA is 1:2, the amount of absorbed SA in the mixture is around 5.4% (Figure S1b, Supporting Information)) in the $Ti_3C_2T_x$ /SA mixture. PDDS was synthesized in the same method, by dissolving 20 mg SA and 30 mg 1,4-diamino-2,5-dichlorobenzene into 30 mL *n*-butanol and reacting for 5 min in the 350-watt microwave. The product, a red powder, was collected by vacuum filtering and drying. The FTIR and Raman spectra of the PDDS, SA and 1,4-diamino-2,5-dichlorobenzene were shown in Figure S18 (Supporting Information).

Fabrication and Test of Gas Sensor: The sensor devices were fabricated by drop-casting 2 µL ethanol dispersion (5 mg mL^{-1}) of the hybrid on the Si/SiO_2 substrate (4 mm × 6 mm × 0.5 mm), with 25 pairs of Au-Ti interdigitated electrodes (electrode distance and width were both 20 µm), to form a sensitive film and dried at room temperature (Figure S19, Supporting Information). The sensing performance of materials was studied in a Linkam THMS600 heating and freezing stage connected to an Agilent 3458A multimeter at 5 V of constant bias. Different concentrations of NH_3, NO, H_2S, CH_4, CO, and H_2 were obtained by Lab view driven mass flow controllers. Dry synthetic air was used as the carrier gas to dilute these gases to the desired concentrations while the operating temperature was maintained at room temperature (25 °C). The total gas flow rate was kept constant at 500 mL min^{-1} in all experiments. The gas response was calculated by $\Delta R \times 100\%/R_0$, where R_0 is the initial sensor resistance before NH_3 exposure and ΔR is the difference between R_0 and the resistance of the sensor exposed to NH_3. To add water vapor to the test gas, additional airflow was bubbled through a water-containing flask and then mixed with the analyte before introducing it into the test chamber. The relative humidity was adjusted by the carrier gas flow rates. The ultimate humidity of the test gas was calibrated via a commercial humidity sensor.

Supporting Information

Supporting Information is available from the Wiley Online Library or from the author.

Acknowledgements

This work was financially supported in part by the University of Oulu (project Entity) and the China Scholarship Council. The authors acknowledge funding from the Academy of Finland under Project No. 311058, 330214, and 325185. The authors thank the personnel of the Centre for Material Analysis at the University of Oulu for providing them with technical assistance.

Conflict of Interest

The authors declare no conflict of interest.

Author Contributions

J.Z. and S.H.H.S. contributed equally to this work. The experiments were designed and carried out by J.Z and S.H.H.S. (J.Z. synthesized the hybrid materials, conducted the XRD, TGA, SEM, electrical and sensor measurements, and analyzed/plotted the data; S.H.H.S. participated in SEM, electrical and sensor measurements along with analyzing the data.) Z.-P. L. and L. C. synthesized the pristine MXene ink. Raman and

FTIR measurements were performed by L.R. and Z.-P. L., respectively. J.Z. and S.H.H.S. drafted the manuscript, which was then discussed and revised by the co-authors.

Data Availability Statement

The data that support the findings of this study are available from the corresponding author upon reasonable request.

Keywords

gas sensing, in situ polymerization, intercalation, microwave reaction, MXene

Received: November 24, 2021
Revised: February 16, 2022
Published online: March 9, 2022

[1] M. Naguib, M. Kurtoglu, V. Presser, J. Lu, J. Niu, M. Heon, L. Hultman, Y. Gogotsi, M. W. Barsoum, *Adv. Mater.* **2011**, *23*, 4248.
[2] A. Levitt, J. Zhang, G. Dion, Y. Gogotsi, J. M. Razal, *Adv. Funct. Mater.* **2020**, *30*, 2000739.
[3] K. Li, M. Liang, H. Wang, X. Wang, Y. Huang, J. Coelho, S. Pinilla, Y. Zhang, F. Qi, V. Nicolosi, *Adv. Funct. Mater.* **2020**, *30*, 2000842.
[4] J. Zhang, Y. Zhao, X. Guo, C. Chen, C.-L. Dong, R.-S. Liu, C.-P. Han, Y. Li, Y. Gogotsi, G. Wang, *Nat. Catal.* **2018**, *1*, 985.
[5] A. Liu, M. Gao, X. Ren, F. Meng, Y. Yang, Q. Yang, W. Guan, L. Gao, X. Liang, T. Ma, *Nanoscale* **2020**, *12*, 10933.
[6] F. Shahzad, M. Alhabeb, C. B. Hatter, B. Anasori, S. M. Hong, C. M. Koo, Y. Gogotsi, *Science (80-.).* **2016**, *353*, 1137.
[7] J. Liu, H. Zhang, R. Sun, Y. Liu, Z. Liu, A. Zhou, Z. Yu, *Adv. Mater.* **2017**, *29*, 1702367.
[8] W. Y. Chen, S.-N. Lai, C.-C. Yen, X. Jiang, D. Peroulis, L. A. Stanciu, *ACS Nano* **2020**, *14*, 11490.
[9] J. Choi, Y. Kim, S. Cho, K. Park, H. Kang, S. J. Kim, H. Jung, *Adv. Funct. Mater.* **2020**, *30*, 2003998.
[10] A. Sinha, H. Zhao, Y. Huang, X. Lu, J. Chen, R. Jain, *TrAC Trends Anal. Chem.* **2018**, *105*, 424.
[11] K. Deshmukh, T. Kovářík, S. K. K. Pasha, *Coord. Chem. Rev.* **2020**, *424*, 213514.
[12] S. J. Kim, H.-J. Koh, C. E. Ren, O. Kwon, K. Maleski, S.-Y. Cho, B. Anasori, C.-K. Kim, Y.-K. Choi, J. Kim, *ACS Nano* **2018**, *12*, 986.
[13] E. Lee, A. VahidMohammadi, B. C. Prorok, Y. S. Yoon, M. Beidaghi, D.-J. Kim, *ACS Appl. Mater. Interfaces* **2017**, *9*, 37184.
[14] E. Lee, D.-J. Kim, *J. Electrochem. Soc.* **2019**, *167*, 037515.
[15] M. Wu, M. He, Q. Hu, Q. Wu, G. Sun, L. Xie, Z. Zhang, Z. Zhu, A. Zhou, *ACS Sens.* **2019**, *4*, 2763.
[16] J. L. Hart, K. Hantanasirisakul, A. C. Lang, B. Anasori, D. Pinto, Y. Pivak, J. T. van Omme, S. J. May, Y. Gogotsi, M. L. Taheri, *Nat. Commun.* **2019**, *10*, 522.
[17] O. Mashtalir, M. Naguib, V. N. Mochalin, Y. Dall'Agnese, M. Heon, M. W. Barsoum, Y. Gogotsi, *Nat. Commun.* **2013**, *4*, 1716.
[18] O. Mashtalir, M. R. Lukatskaya, A. I. Kolesnikov, E. Raymundo-Pinero, M. Naguib, M. W. Barsoum, Y. Gogotsi, *Nanoscale* **2016**, *8*, 9128.
[19] A. Al-Temimy, B. Anasori, K. A. Mazzio, F. Kronast, M. Seredych, N. Kurra, M.-A. Mawass, S. Raoux, Y. Gogotsi, T. Petit, *J. Phys. Chem. C* **2020**, *124*, 5079.
[20] M. Boota, B. Anasori, C. Voigt, M. Zhao, M. W. Barsoum, Y. Gogotsi, *Adv. Mater.* **2016**, *28*, 1517.
[21] Z. Li, C. Ma, Y. Wen, Z. Wei, X. Xing, J. Chu, C. Yu, K. Wang, Z.-K. Wang, *Nano Res.* **2020**, *13*, 196.
[22] L. Zhao, Y. Zheng, K. Wang, C. Lv, W. Wei, L. Wang, W. Han, *Adv. Mater. Technol.* **2020**, *5*, 2000248.
[23] Y. Zhou, Y. Wang, Y. Wang, X. Li, *Anal. Chem.* **2020**, *92*, 16033.
[24] L. Zhao, K. Wang, W. Wei, L. Wang, W. Han, *InfoMat* **2019**, *1*, 407.
[25] X. Wang, K. Sun, K. Li, X. Li, Y. Gogotsi, *Chinese Chem. Lett.* **2020**, *31*, 1018.
[26] H. Tai, Z. Duan, Z. He, X. Li, J. Xu, B. Liu, Y. Jiang, *Sensors Actuators B Chem.* **2019**, *298*, 126874.
[27] S. H. Lee, W. Eom, H. Shin, R. B. Ambade, J. H. Bang, H. W. Kim, T. H. Han, *ACS Appl. Mater. Interfaces* **2020**, *12*, 10434.
[28] T. He, W. Liu, T. Lv, M. Ma, Z. Liu, A. Vasiliev, X. Li, *Sensors Actuators B Chem.* **2020**, 129275.
[29] Z. Yang, L. Jiang, J. Wang, F. Liu, J. He, A. Liu, S. Lv, R. You, X. Yan, P. Sun, *Sensors Actuators B Chem.* **n.d.**, *326*, 128828.
[30] H.-J. Koh, S. J. Kim, K. Maleski, S.-Y. Cho, Y.-J. Kim, C. W. Ahn, Y. Gogotsi, H.-T. Jung, *ACS Sens.* **2019**, *4*, 1365.
[31] N. C. Osti, M. Naguib, A. Ostadhossein, Y. Xie, P. R. C. Kent, B. Dyatkin, G. Rother, W. T. Heller, A. C. T. Van Duin, Y. Gogotsi, *ACS Appl. Mater. Interfaces* **2016**, *8*, 8859.
[32] E. S. Muckley, M. Naguib, H.-W. Wang, L. Vlcek, N. C. Osti, R. L. Sacci, X. Sang, R. R. Unocic, Y. Xie, M. Tyagi, *ACS Nano* **2017**, *11*, 11118.
[33] X. Li, J. Xu, Y. Jiang, Z. He, B. Liu, H. Xie, H. Li, Z. Li, Y. Wang, H. Tai, *Sensors Actuators B Chem.* **2020**, 128144.
[34] L. Jin, C. Wu, K. Wei, L. He, H. Gao, H. Zhang, K. Zhang, A. M. Asiri, K. A. Alamry, L. Yang, *ACS Appl. Nano Mater.* **2020**, *3*, 12071.
[35] M. Boota, M. Pasini, F. Galeotti, W. Porzio, M.-Q. Zhao, J. Halim, Y. Gogotsi, *Chem. Mater.* **2017**, *29*, 2731.
[36] S. H. Overbury, A. I. Kolesnikov, G. M. Brown, Z. Zhang, G. S. Nair, R. L. Sacci, R. Lotfi, A. C. T. van Duin, M. Naguib, *J. Am. Chem. Soc.* **2018**, *140*, 10305.
[37] J. Wang, L. Liu, S. Jiao, K. Ma, J. Lv, J. Yang, *Adv. Funct. Mater.* **2020**, *30*, 2002595.
[38] G. B. Dudley, A. E. Stiegman, M. R. Rosana, *Angew. Chem., Int. Ed.* **2013**, *52*, 7918.
[39] X. Xiao, X. Cheng, X. Hou, J. He, Q. Xu, H. Li, N. Li, D. Chen, J. Lu, *Small* **2017**, *13*, 1602190.
[40] C. Yu, H.-Z. Lin, J. Zhou, X.-F. Cheng, J.-H. He, H. Li, Q.-F. Xu, N.-J. Li, D.-Y. Chen, J.-M. Lu, *J. Mater. Chem. A* **2020**, *8*, 1052.
[41] J. Zhou, X. F. Cheng, B. J. Gao, C. Yu, J. H. He, Q. F. Xu, H. Li, N. J. Li, D. Y. Chen, J. M. Lu, *Small* **2019**, *15*, 1803896.
[42] J. Zhou, T. Järvinen, O. Pitkänen, Z. Kónya, A. Kukovecz, K. Kordas, *Nanotechnology* **2021**, *32*, 185502.
[43] M. Boota, C. Chen, L. Yang, A. I. Kolesnikov, N. C. Osti, W. Porzio, L. Barba, J. Jiang, *Chem. Mater.* **2020**, *32*, 7884.
[44] C. R. Chenthamarakshan, A. Ajayaghosh, *Chem. Mater.* **1998**, *10*, 1657.
[45] V. S. Talens, D. M. M. Makurat, T. Liu, W. Dai, C. Guibert, W. E. M. Noteborn, I. K. Voets, R. E. Kieltyka, *Polym. Chem.* **2019**, *10*, 3146.
[46] R. J. Stokes, A. Ingram, J. Gallagher, D. R. Armstrong, W. E. Smith, D. Graham, *Chem. Commun.* **2008**, 567.
[47] A. Sarycheva, Y. Gogotsi, *Chem. Mater.* **2020**, *32*, 3480.
[48] K. G. Neoh, E. T. Kang, K. L. Tan, *Synth. Met.* **1991**, *40*, 341.
[49] K. L. Tan, B. T. G. Tan, E. T. Kang, K. G. Neoh, *J. Chem. Phys.* **1991**, *94*, 5382.
[50] K. Raagulan, R. Braveenth, H. J. Jang, Y. Seon Lee, C.-M. Yang, B. Mi Kim, J. J. Moon, K. Y. Chai, *Materials (Basel).* **2018**, *11*, 1803.
[51] S. Kim, J. Lee, S. Doo, Y. C. Kang, C. M. Koo, S. J. Kim, *ACS Appl. Nano Mater.* **2021**, *4*, 14249.

[52] D. Wang, D. Zhang, Y. Yang, Q. Mi, J. Zhang, L. Yu, *ACS Nano* **2021**, *15*, 2911.
[53] T. Yang, L. Gao, W. Wang, J. Kang, G. Zhao, D. Li, W. Chen, H. Zhang, *Nano-Micro Lett.* **2021**, *13*, 63.
[54] X. Li, T. He, in *ECS Meet. Abstr.*, IOP Publishing, **2020**, p. 2460.
[55] Q. Sun, J. Wang, X. Wang, J. Dai, X. Wang, H. Fan, Z. Wang, H. Li, X. Huang, W. Huang, *Nanoscale* **2020**, *12*, 16987.
[56] E. Wongrat, T. Nuengnit, R. Panyathip, N. Chanlek, N. Hongsith, S. Choopun, *Sensors Actuators B Chem.* **2021**, *326*, 128983.
[57] H.-Y. Li, C.-S. Lee, D. H. Kim, J.-H. Lee, *ACS Appl. Mater. Interfaces* **2018**, *10*, 27858.
[58] M. Xue, F. Li, D. Chen, Z. Yang, X. Wang, J. Ji, *Adv. Mater.* **2016**, *28*, 8265.
[59] A. Liu, S. Lv, L. Jiang, F. Liu, L. Zhao, J. Wang, X. Hu, Z. Yang, J. He, C. Wang, *Sensors Actuators B Chem.* **2021**, *332*, 129444.
[60] Zhengzhou Winsen Electronics Technology Co., Ltd., Ammonia Gas Sensor (Model: MQ137) Manual, https://www.winsen-sensor.com/d/files/semiconductor/mq137.pdf (accessed: February 2022).
[61] Figaro USA, Inc. TGS 826 – for the Detection of Ammonia, Product Information, https://www.figarosensor.com/product/docs/TGS%20826%20%2805_04%29.pdf (accessed: February 2022).
[62] B. A. J. Lechner, Y. Kim, P. J. Feibelman, G. Henkelman, H. Kang, M. Salmeron, *J. Phys. Chem. C* **2015**, *119*, 23052.
[63] L. T. Duy, T. Q. Trung, V. Q. Dang, B. Hwang, S. Siddiqui, I. Son, S. K. Yoon, D. J. Chung, N. Lee, *Adv. Funct. Mater.* **2016**, *26*, 4329.
[64] P. Khakbaz, M. Moshayedi, S. Hajian, M. Soleimani, B. B. Narakathu, B. J. Bazuin, M. Pourfath, M. Z. Atashbar, *J. Phys. Chem. C* **2019**, *123*, 29794.
[65] J. Zhou, H. Lin, X. F. Cheng, J. Shu, J. H. He, H. Li, Q. F. Xu, N. J. Li, D. Y. Chen, J. M. Lu, *Mater. Horiz.* **2019**, *6*, 554.
[66] M. Alhabeb, K. Maleski, B. Anasori, P. Lelyukh, L. Clark, S. Sin, Y. Gogotsi, *Chem. Mater.* **2017**, *29*, 7633.